Submitted to Int. J. Remote Sensing (Jan 2002), Accepted Sept 2002

Single frequency processing of GPS radio occultations

M. de la Torre Juárez, G.A. Hajj, E.R. Kursinski[†], D. Kuang, A.J. Mannucci, L.J. Romans
M-S 238-600, Jet Propulsion Laboratory; Pasadena, CA 91109. U.S.A.
[†] Also at Dept. of Atmospheric Sciences, University of Arizona, Tucson, AZ, U.S.A.

September 25, 2002

Abstract

Tracking of the radio signals broadcast by the Global Positioning System (GPS) satellites as they are occulted from a GPS receiver by the Earth's atmosphere can provide high resolution vertical profiles of atmospheric refractivity, temperature and water vapour. Most implementations of this radio occultation technique use the 2 GPS frequencies to correct for ionospheric effects. However, during most soundings, one of the frequencies is degraded by the introduction of the so-called Anti-Spoofing (AS) encryption mode. An alternative retrieval method is discussed in this work for periods when only one of the two frequency signals has good quality. This method uses only the frequency with higher signal-to-noise ratio. We illustrate the quality of the atmospheric profiles obtained from such single frequency retrievals using GPS/MET data from the periods where the AS was turned off and the two frequencies were available. The results enable to ensure the quality of a climate record of thousands of radio occultations collected by GPS/MET during the period with AS encryption, and data processing of future missions with similar constraints, like IOX, can be performed.

Keywords: Atmosphere, Climate, GPS, Remote Sensing, Occultations.

Author to whom correspondence should be sent:
Manuel de la Torre Juárez
M-S 238-600; JPL; 4800 Oak Grove Dr.
Pasadena, CA 91109-8099.
e-mail: mtj@jpl.nasa.gov
Phone: +1 (818) 354-4548
Fax: +1 (818) 393-4965

1 Introduction

Radio Occultation profiling of atmospheric temperature, pressure, geopotentials and water vapour using the signal broadcast by the Global Positioning System (GPS) has been proposed for a systematic monitoring of weather and climate (*Yunck et al.* 1988, e.g.). Since then, The GPS-MET mission demonstrated the proof of concept, and more recent missions such as OERSTED, CHAMP, SAC-C, and the most recent IOX have carried instruments that enable this type of sounding. The accuracy of these soundings has been validated favourably against other remote sounding techniques, models, and radiosondes (*Kursinski et al.* 2000; *Anthes et al.*, 2000, e.g. and references therein). During all the missions, the signal transmitted by the GPS satellites has been usually encrypted by the inclusion of the Anti-Spoofing (AS) code by the US Department of Defence. When the AS code is turned on, the quality of the extracted carrier phase is degraded for one of the GPS frequencies, but signals broadcast at two frequencies are typically needed to separate ionospheric from atmospheric contributions to the signal phase delay. The degradation of one frequency signal may thus introduce errors in the resulting atmospheric profiles.

AS was turned off during four periods of the GPS/MET mission: from 1995-04-18 to 1995-05-11, from 1995-06-19 to 1995-07-11, from 1995-10-10 to 1995-11-01, and from 1997-02-02 to 1997-02-03. During these 72 days, the signal to noise ratio (SNR) of the second frequency signal in the occulting link is high in GPS/MET as is shown in figure 1a. The amplitude of the degraded frequency (L2-SNR) starts at a high value, and as the signal starts traversing the denser troposphere, the L2-SNR decays. This behaviour is expected during a typical atmospheric radio occultation. A high L2-SNR permits a reliable separation of the ionospheric and atmospheric contributions to the delay using a *dual frequency* method described below. For the sake of comparison, we have included also an average of the L2-SNR during the AS-on periods for GPS/MET, CHAMP, and OERSTED. The differences in the amplitudes of the L2-SNR are

caused by improvements in the instrumentation. CHAMP and SAC-C are carrying "Blackjack" type receivers. GPS/MET, OERSTED and IOX were carrying or carry Turborogue receivers. It appears clear that, while for CHAMP the second frequency exhibits a high SNR and its temporal behaviour resembles the GPS/MET L2-SNR without AS, OERSTED and GPS/MET with AS-on show a very low L2-SNR and the temporal behaviour differs from the shape of CHAMP or the AS-off periods of GPS/MET. As a consequence the type of processing described here is applied on GPS/MET and OERSTED and is conceived for IOX.

The purpose of this work is to describe the implementation of an atmospheric profiling method that only uses the stronger Clear Acquisition (CA) signal available on the L1 frequency, and assess the quality of the results. Atmospheric profiles obtained from CA-only and from dual frequency retrievals were compared for this purpose from GPS/MET data during the days when the AS was turned off.

1.1 Occultation geometry

GPS-atmospheric radio occultations are active limb soundings in which a GPS receiver aboard a Low Earth Orbiting satellite (LEO) tracks the coherent signal broadcast by the GPS satellites as they occult or rise behind the Earth's atmosphere. The signal is transmitted by the GPS satellites at two carrier frequencies: $f_1 = 1,575.42 = 154 \times 10.23$ MHz and $f_2 = 1,227.6 = 120 \times 10.23$ MHz. These frequencies are not absorbed by water and can thus penetrate through clouds. As the GPS signals traverse the atmosphere, they are curved by the atmospheric density gradients across the ray path following Fermat's principle. This bending lengthens the ray-path introducing a delay in the phase of the signal which can be measured. The delay can be used to calculate the bending α of the signal as a function of the ray impact parameter. The impact parameter a is defined as the perpendicular distance between the centre of the local ray curvature near the tangent point of the ray and the asymptotic straight line followed by the ray as it approaches the atmosphere. For an atmosphere which is locally spherically symmetric,

there is a unique relationship between the bending $\alpha(a)$ and the atmospheric refractive index $n(r)$ so that the bending can be used in turn to derive the refraction index of the atmospheric layer traversed by the ray(*Kursinski et al.* 2000, or references therein).

During each occultation the GPS signal is tracked as it moves vertically in the atmosphere, so that occultations return vertical refraction index profiles with a vertical resolution given by the Fresnel diffraction limit which ranges typically from 100 m to 1000 m for receivers on LEOs. This vertical resolution is higher than with any other remote sounding technique and can actually be improved as discussed in Gorbunov (2001).

The precision in the bending angle measurements depends on the accuracy with which the phase delay is measured at the receiver. A precise phase delay is obtained by calibrating the receiver clock errors by tracking the clock from a second GPS satellite which is not occulting behind the atmosphere, so that its signal only traverses the ionospheric layers above the LEO and can be corrected by a simple ionospheric correction method. This non-occulting GPS link will be referred to as the non-occulting link, while the GPS signal which leads to the atmospheric profiles after occulting behind the atmosphere will be referred to as the occulting link.

1.2 Ionospheric Total Electron Content from phase and range delays

The phase and group velocities of a GPS signal traversing the atmosphere and ionosphere undergoes delays given by:

$$L_k^* = -\frac{c}{f_k}\Phi_k = \rho + \eta_k - \frac{I}{f_k^2} + \epsilon_k^t + \epsilon_k^r + \nu_k + B_k$$

$$P_k^* = \rho + \eta_k + \frac{I}{f_k^2} + \tau_k^t + \tau_k^r + \mu_k$$

Where k is the subindex indicating the carrier frequency. L_1^* and L_2^* are the phase delays measured for the first and second carrier frequencies, P_1^* and P_2^* are the corresponding pseudo-ranges or group velocity delays, c is the speed of light, f_k is the frequency of the signal, ρ is the delay introduced by the geometric distance between transmitter and receiver, η_k is the delay

caused by the refraction of the ray path in the neutral atmosphere, I_k/f_k^2 is the signal delay caused by the ionosphere, ϵ_k^t and τ_k^t represent the hardware delay and clock shifts on phase and range at the transmitter, ϵ_k^r and τ_k^r represent the hardware delay and clock shifts on phase and range at the receiver, ν_k and μ_k represent the measurement noise that includes thermal noise and local multi-path, and B_k is a bias in the phase measurement which is assumed to be a constant integer number of cycles for each occultation ($B_k = n_k\lambda_k$, with n_k two unknown integers). The ionospheric term I_k is proportional to the integral of the total electron content TEC_k along the ray-path. Since signals with different frequencies may follow different paths, the ionospheric delay I_k differs for each signal used in a dual frequency retrieval. The difference introduced by these two paths has been analysed and described as small (*Syndergaard* 2000, e.g. and references therein). One can take therefore approach $I_k \simeq I$ as frequency independent to a first order of approximation. In the single frequency method, such a difference does not exist, but there is a greater uncertainty in the pseudo-range measurements P_k^*. The prefactor c/f_k is typically used to express the delays in units of length.

For atmospheric profiling, a calibration step is required to subtract the geometric distance ρ, the clock errors ϵ_k^t, ϵ_k^r, τ_k^r and τ_k^t, and the bias B_k so that the calibrated signals L_k, P_k contain only the ionospheric and atmospheric delays, that is: $L_k = \eta_k - \frac{I}{f_k^2}$, and $P_k = \eta_k + \frac{I}{f_k^2}$. [1] From the latter identities, if both frequency signals are available, the ionospheric contribution can be obtained from

$$L_1 - L_2 = (\frac{f_1^2}{f_2^2} - 1)\frac{I}{f_1^2}, \quad thus \quad \frac{I}{f_1^2} = a_0(L_1 - L_2) \tag{1}$$

where $1/a_0 = f_1^2/f_2^2 - 1$. On the other hand, when only one frequency is available, one can also estimate I from:

$$P_1 - L_1 = 2\frac{I}{f_1^2}, \quad and\ thus \quad \frac{I}{f_1^2} = 0.5(P_1 - L_1) \tag{2}$$

In a dual frequency retrieval, the ionospheric contribution is calculated using 1, while for

[1] The measurement noise will be neglected from this point on.

a single frequency retrieval, 2 is used on the CA signal which has the carrier frequency f_1. A comparison of the ionospheric terms obtained by both methods is shown in figure 1b as a function of time for two typical occultations. For GPS/MET, the values for the Ionospheric correction using the CA-only or single frequency method are given every second while the dual frequency method returns a correction term every 0.02 sec. This is due to the fact that the pseudo-range data were acquired with a 1Hz frequency while the phase delays were acquired with a 50 Hz frequency. The occultation in 1995 shows a typical result for the AS-off period, and the occultation in 1996 corresponds to a period when the AS was turned on. It is clear that the difference between the single and dual frequency ionospheric terms is small in the AS-off period, and large in the AS-on period of 1996. This shows that an estimate of the ionosphere using the dual-frequency correction is inappropriate for GPS/MET when the AS was on due to poor tracking of the L2.

The errors shown in figure 1b for the ionospheric delay estimate are propagated to the calculation of the atmospheric delay of the occulting signal. This can cause significant degradation of the atmospheric profiles during the AS-on periods. Similarly, the estimate of the clock errors needed to obtain the calibrated signal L_k from the observed L_k^*, can be affected by errors on the estimate of the ionospheric term for the non-occulting link since, during the calibration, delays introduced by clock errors are calculated by obtaining first the geometrical distance and then the ionospheric contribution to the non-occulting link. The single frequency method will be described next for the clock calibrations that use the orbit solutions and the ionospheric TEC along the non-occulting link.

2 Dual versus single frequency calibrations

To obtain the atmospheric delay of the occulting signal one needs to subtract the satellite positions and the clock errors from the observed phase delays. This procedure is called the signal calibration. The present section describes the differences observed in the results of the

signal calibrations by both, the single and the dual processing methods.

Since radio occultation profiling derives atmospheric refractivity from the signal bending angles and these are obtained from the time derivatives of the phase delays (*Kursinski et al.* 2000, e.g.), the comparisons between dual and single frequency delays will be discussed in terms of these time derivatives. Equally, the orbit solutions will be compared in terms of their calculated velocities rather than the positions.

2.1 Orbits

The reduced dynamic approach (Wu et al., 1991) is used for calculating the GPS/MET orbits. In order to correct for the ionospheric delay in the single frequency measurement, the BENT ionospheric model is used to calculate the vertical TEC and a scale factor is estimated from the actual data fit. The quality of the orbit determined with single frequency data is validated in the way described by Bertiger and Wu (1996). AS-off days were chosen for which good quality dual frequency measurements are available. Accurate GPS/MET orbit solutions are computed first using the ionosphere free combination of the dual frequency measurements. These dual frequency orbit solutions are taken as the truth orbit. Then single frequency measurements are used to compute the single frequency orbit solutions. The single frequency orbit solutions are compared with the truth orbit, providing an evaluation of the quality of the single frequency orbit solutions.

Thirty-one days from the 1995 AS-off periods were used to assess the quality of single frequency orbit solutions. Statistics were performed on the solutions for the time intervals for which there were valid measurement data. The statistics of the differences in the solutions are illustrated in table I and indicate that the orbit velocity agrees to better than millimetre/second. The components shown are the along-track v_l, across-track v_c and vertical v_h velocity components.

2.2 Clock errors

Transmitter GPS-satellite clocks are calibrated by comparing them against ground station clocks whose errors are not significant. The error in the occulting receiver's clock is obtained by measuring the signal sent by a non-occulting GPS-satellite to the receiver. This non-occulting signal is going only through vacuum and the ionosphere. The ionospheric delay along the non-occulting link is therefore calculated using either equation 1 or 2. Differences in the estimate of the ionospheric delay of the non-occulting signal cause differences in the calculated clock errors ϵ_k^r and τ_k^r. These result in a different value of the calibrated occulting signal from which the atmospheric profiles must be derived. Differences are expected to be more significant when the ionosphere displays a higher variability. The highest Ionospheric variabilities were measured for the 1995 AS-off period in May 4th and 5th. The values of the global ionospheric index A_p, a typical measure of geomagnetic variability often associated with disturbed ionospheric conditions, were $A_p = 35$, and $A_p = 43$ respectively. For the sake of comparison, table II shows the statistics of A_p throughout the years of the GPS/MET mission as well as for 1999 and 2000 where we have entered the period of maximum solar flux. Within all of 1995, 17 days had $A_p \geq 35$ and 7 days had $A_p \geq 43$. Within the years 1995-1997, the numbers increase to 29 days with $A_p \geq 35$ and 12 days with $A_p \geq 43$. Maybe more important for the relevance of the present work is that even though 1995 was not a solar maximum year, the 4th. and 5th. of May reached about two to three times the typical A_p values for the year 2000.

The occultation phase delay was recorded for GPS/MET at a higher data rate (50 Hz) than the 1Hz rate of the pseudo-ranges. The single frequency method can synthesise the ionospheric correction at a higher rate by assuming that the ionospheric delay can be modelled by a polynomial function between 1-second measurements. This was done by fitting the $P_1 - L_1$ differences to a single polynomial expression over the entire length of the occultation (typically ~ 2 min). Since the optimal truncation degree of such an expansion is not known, we have made statistical

comparisons using polynomials of orders 1 to 8. Figure 1b also shows that a modelling approach has an additional advantage: the ionospheric delays obtained with the single frequency method appear noisier than the dual frequency result and the noise is smoothed by the fit to a model. The statistics of the differences in the calibrated phase rates are presented in table III for the expansions of orders 1, 2, and 4. The results for the 8th order showed anomalous oscillations trying to recreate the high frequency variability caused by the noise in the range measurement. Table III shows the dual-single phase rates in mm/s for 130 successful calibrations obtained from 1995-05-04 and 1995-05-05.

Assuming the dual frequency retrieval as the truth value, the first degree polynomial appears to provide the best model of the ionospheric delay. A small number of cases were also found where a higher degree would have captured better some structure which was apparent in the dual frequency ionospheric delay. This situation is illustrated in figure 1b where the ionospheric term for the AS-on period appears to be closer to a second order polynomial than to a line. Such nonlinear structures were however the exception.

Another effect of the degree of the polynomial model is the introduction of some trends. Figures 2 show scatter plots of the differences between the time derivative of the phase delays in the dual minus the single frequency calibration. For some occultations the differences showed a nonlinear trend towards the end of the occultation. This trend is absent in the linear expansion. For this reason the clock calibration was made using a linear fit.

3 Atmospheric profiles

Atmospheric profiles were retrieved from the phase delays in the occulting link after subtracting the geometric and ionospheric delays. On the occulting link, the pseudo-range data needed for the ionospheric correction 2 were again available once per second, and an interpolation method was needed like for the non-occulting link, to construct a 50 Hz signal. One feature of the occulting link is that it is traversing the troposphere and two sections of the ionosphere

that are more distant from each other than in the non-occulting link. The distance between the ionospheric regions delaying the signal grows as the occultation progresses and they may reach points where they are totally disconnected. As a consequence, the signal delay is affected by the intrinsic ionospheric variability in very distant regions. This delay may therefore be poorly captured with a linear approach. On the other hand, a high order polynomial expansion increases the risk of incorporating noise into the fit to the data. An approach to solve this is to fit to quasi-linear models within moving temporal windows. This was done and the effect of the window length is discussed next.

Two atmospheric variables were compared for this study: atmospheric refractivity N, and temperature T. A typical profile comparison is shown in figures 3a and 3b for the refractivity and temperature profiles as a function of height. In the single frequency method the ionospheric correction was based on equation 2 with 10 and 30 second windows, while the dual frequency retrievals were obtained using the ionospheric correction suggested by Vorob'ev & Karsil'nikova (1994) that linearly combines the bending angles at each frequency instead of the phase differences 1.

The reason for the choice of these 2 variables is that while the retrieval of N is independent of model initialisation, the T profiles used for the comparisons were retrieved using model initialisation. As a consequence, errors in N reflect the effect of the model-independent parameters in our retrieval while errors in T reflect the effect of model constraints on the measurement. The model will be shown to have a clear effect at high altitudes.

The retrievals shown in figures 3 are very similar and some difference appears only above the tropopause where the ten second moving window differs more from the dual frequency result than the 30 second window. A statistical comparison was carried out for 131 profiles with ten sec window and 121 profiles of the 30 sec window. The statistics are shown in figures 4 as a function of height. The occultations chosen occurred within 2 days of the AS-off period: 1995-07-01 and

1995-07-03. The mean difference in fractional refractivity remains under 0.7 % up to 40 km, growing with altitude. Its standard deviation remains under one percent below 27 km. and grows above to reach four and a half percent near 40 km. Temperature differences are affected by how consistent is the measured refractivity at the top with the temperature of the model. The mean differences between the single and dual temperature profiles is less than half degree K below 24 km. It grows with height for the 30 sec windowing method while it remains below three quarters of a degree K level for the ten sec windowing. Above 32 km the temperature differences decrease, unlike the refractivity, because the profiles are initialised such that they have the same temperature at the maximum height of the model. This initialisation forces the difference to go to zero at the maximum height of the model.

3.1 Error minimisation in the refractivity to temperature conversion

Figures 4 illustrate that the statistical differences in refractivities and temperatures have different behaviours at high altitudes. This difference can be understood from the method to derive temperature from refractivity. Next we address the source of this difference and how do we expect to minimise temperature retrieval errors.

Refractivity N of radio waves in a moist atmosphere relates to temperature by the expression:

$$N = a_1 \frac{p}{T} + a_2 \frac{e}{T^2} = R \left(\frac{a_1}{M_a} \rho + \frac{a_2}{M_v} \frac{\rho_v}{T} \right)$$

where T is temperature in Kelvin, p is pressure in millibar, e is water vapour pressure in millibar, ρ is density of air, ρ_v is the density of water vapour, R is the gas constant, M_a is the molecular weight of air, M_v is the molecular weight of water vapour, $a_1 = 77.6$ K/mbar, and $a_2 = 3.73 \times 10^5$ K^2/mbar. In hydrostatic balance, $p(z) - p(z_0) = -\int_{z_0}^{z} \rho(\vec{r}) g(\vec{r}) dz$, where $g(\vec{r})$ is the gravity acceleration field, $\vec{r}$ is the position vector, and z is the vertical coordinate.

In the upper troposphere and lower stratosphere the contribution of water vapour to refractivity can be neglected, and thus the thermodynamical variables in this dry part of the

atmosphere can be obtained from:

$$\rho(\vec{r}) = \frac{M_a}{a_1 R} N \quad \rightarrow \quad p(z) = p(z_0) - \frac{M_a}{a_1 R} \int_{z_0}^{z} N g dz \quad \rightarrow \quad T(z) = \frac{M_a p}{R\rho} = \frac{a_1 p(z_0)}{N} - \frac{M_a}{RN} \int_{z_0}^{z} N g dz$$

A single frequency retrieval will capture a refractivity that differs from the "true" (dual frequency) value by a magnitude ΔN. As a consequence, the temperature error ΔT can be obtained from:

$$T + \Delta T = \frac{a_1 p(z_0)}{N + \Delta N} - \frac{M_a}{R(N + \Delta N)} \int_{z_0}^{z} g(N + \Delta N) dz =$$

$$= \left[\frac{a_1 p(z_0)}{N} - \frac{M_a}{RN} \int_{z_0}^{z} g(N + \Delta N) dz \right] \left[1 - \frac{\Delta N}{N} + O\left(\frac{\Delta N}{N} \right)^2 \right] =$$

$$= \left(T - \frac{M_a}{RN} \int_{z_0}^{z} g \Delta N dz \right) \left[1 - \frac{\Delta N}{N} + O\left(\frac{\Delta N}{N} \right)^2 \right]$$

subtracting the true T value thus leads to,

$$\Delta T = -T \frac{\Delta N}{N} - \frac{M_a}{RN} \int_{z_0}^{z} g \Delta N dz \left(1 - \frac{\Delta N}{N} \right) + O\left(\frac{\Delta N}{N} \right)^2$$

The dominant contributions to the temperature difference are related by the fractional refractivity difference $\Delta N/N$. Further, one can see that to leading order a constant refractivity bias will cause temperature biases of opposite sign. This happens because the sign of ΔT is opposite to the sign of ΔN to leading order.

One can now observe two features in figures 4(a-b). The first one is that the different shapes in temperature and refractivity errors are due to the fact that while the difference in refractivity increases with height, refractivity itself decreases. This explains why the standard deviation of the temperature differences increases in a more pronounced manner than refractivity differences until altitudes near 30 km. The second feature is that the refractivity and temperature biases appear mostly positive (dual retrievals being warmer than single frequency retrievals), both with the same sign in apparent contradiction with our previous expression. The same sign and the decay in temperature differences above 30 km have its explanation in an extra consideration that can be used to lessen the temperature errors.

The extra consideration relies on noticing that a bias in refractivity can be diminished by initialising the temperature with the same value temperature $T(z_0)$ at the top boundary instead of using pressure initialisation for both retrieval methods. To see this, notice that $a_1 p(z_0) = N(z_0)T(z_0)$, and therefore the boundary condition can be taken by fixing the temperature. The error is given in that case by:

$$T + \Delta T|_{T(z_0)} = T(z_0)\frac{N(z_0) + \Delta N(z_0)}{N + \Delta N} - \frac{M_a}{R(N + \Delta N)} \int_{z_0}^{z} g(N + \Delta N)dz$$

where $\Delta T|_{T(z_0)}$ indicates the temperature error caused by initialisation with a common $T(z_0)$. A bias in refractivity at the top automatically causes a difference with the previous expression given by

$$\Delta T|_{T(z_0)} = \Delta T|_{p(z_0)} + T(z_0)\frac{\Delta N(z_0)}{N}\left(1 - \frac{\Delta N}{N}\right) + O\left(\frac{\Delta N}{N}\right)^2$$

where $\Delta T|_{p(z_0)}$ is the temperature error when the initialisation is by a common $p(z_0)$ (the first expression above). Because, as discussed above, constant biases in ΔN result in biases of opposite sign for $\Delta T|_{p(z_0)}$, the error obtained with temperature initialisation is closer to zero than with pressure initialisation unless the absolute value of the dominant term, $T(z_0)\Delta N(z_0)/N$, becomes larger than twice the temperature error in $\Delta T|_{p(z_0)}$. This situation is very unlikely. At z_0 the temperature error must be zero for temperature initialisation and, because refractivity decreases with height, for a constant bias, this term decreases with height more rapidly than the non-integral contribution to $\Delta T|_{p(z_0)}$. The temperature initialisation has been used to obtain figures 3 and 4, and explains why the temperature differences decay above 30 km as well as the fact that the refractivity differences do not necessarily have opposite sign to the temperature differences.

A last error check was applied on the final retrieved profiles. Below the tropopause occultation profiles are required to differ by less than ten Kelvin from the temperature profiles in the model used for initialisation, and less than 20 K above. This condition has proven sufficient to detect profiles that have anomalous characteristics where something may have gone wrong in the

data quality. The remaining profiles were used for the statistics and one can see that their deviation from the model is much smaller than the ten Kelvin that set the quality control criterion. The differences between the radio occultations processed in the single frequency approach and a global circulation model (ECMWF analysis) are illustrated in figures 5 using 610 GPS/MET occultations from the year 1996. The processing for these occultations used 10 second windows and the type of quality control described above. The ECMWF model values were interpolated to the locations and times of the occultations for the comparison. Figures 5 show that the occultations appear to retrieve colder temperatures, but in the mean, sub-Kelvin accuracy is achieved in the altitude range between four and 24 km, like with dual frequency retrievals. The tracking quality at lower altitudes was poorer in the GPS/MET receiver making the statistical comparisons at these heights look worse. An new type of receiver more appropriate for tracking at these lower altitudes, and new retrieval methods are currently under development. As described in this section, above 24 km the atmosphere is very dry and the error is caused by the fractional difference in refractivity values combined with the requirement that the temperature integral in the occultation is fixed to match the model's temperature at the top. This error could be the source of the bias towards colder temperatures. One way to eliminate this error would be to initialise the temperature integral with the value that the model would have if it had the same refractivity as the data, but this approach is infeasible at the moment.

4 Conclusions

Based on the statistical comparisons presented here, one can address now the quality of the single frequency profiles. The standard deviations of fractional refractivity differences between the dual and the single frequency retrievals shown in figure 4b, are close to or less than the refractivity errors estimated for the dual frequency processing with a large ionosphere, and at low latitude (*Kursinski et al.* 2000), and less than differences of the dual frequency with the NCEP or ECMWF model outputs (*Kursinski et al.* 2000; *Anthes et al.*, 2000, e.g.). Similarly

for the temperature differences. The standard deviations in figure 4d are close to or less than the temperature errors predicted for a large ionosphere and a low latitude in (*Kursinski et al.* 2000), and smaller than previous comparisons with model output (*Kursinski et al.* 2000; *Anthes et al.*, 2000, e.g.). Figures 4a-d also show what the main challenges are for possible improvements of the single frequency retrievals: The 10 sec averaging window produces a result closer to the dual retrieval below 25 km, while the 30 sec averaging window shows better results at higher altitudes. This is caused by the low refractivity values at high altitudes, where a small difference has a higher weight, and therefore the effect of the measurement noise, caused by the noisy pseudo-range measurement, is more significant. A 30 sec window smoothes this noise better than the 10 sec window, but, on the other hand, a 30 sec window may be masking some tropospheric structure which is being captured by a 10 sec window.

Acknowledgments

The research described in this work was performed at the Jet Propulsion Laboratory, California Institute of Technology, supported by the National Aeronautics and Space Administration. We would would like to thank the GPS/MET Principal Investigator, Randolph Ware, and program manager, Mike Exner for access to the raw GPS/MET data. We would like to thank the CHAMP project manager, Chris Reigber, for access to the raw CHAMP data, and the Oersted principal investigator, Per Hoeg, for access to the Oersted data. The ECMWF data have been provided by UCAR.

References

ANTHES, R.A., ROCKEN, C., and KUO, Y.-H., 2000, Applications of COSMIC to Meteorology and climate. Terr. Atmos. and Ocean. Sci., **11**, 115–156.

BERTIGER, B.I. and WU, S.C., 1996, Single frequency GPS orbit determination for low Earth orbiters, proceedings of ION GPS-96, Kansas City, MO.

FJELDBO, G., KLIORE, A.J., ESHLEMAN, V.R., 1971, The neutral atmosphere of Venus as studied with the Mariner V radio occultation experiments. Astronom. J., **76**, 123-140.

GORBUNOV, M.E., 2001, Radioholographic methods for processing radio occultation data in multipath regions. Scientific Report 01-02, Danish Meteorological Institute, DMI Copenhagen 200.

HOFMAN-WELLENHOF, B., LICHTENEGGER, H., and COLLINS, J., 1992, GPS Theory and Practice. Springer Verlag.

HARDY, K.R., HAJJ, G.A., and KURSINSKI, E.R., 1994, Accuracies of atmospheric profiles obtained from GPS occultations. Int. J. of Satellite Comm., **12**, pp. 463–473.

KURSINSKI, E.R., HAJJ, G.A., HARDY, K.R., ROMANS, L.J., and Schofield, J.T., 1995, Observing tropospheric water vapor by radio occultation using the global positioning system. Geophys. Res. Letters, **22**, pp. 2365–2368.

KURSINSKI, E.R., HAJJ, G.A., BERTIGER, W.I., LEROY, S.S., MEEHAN, T.K., ROMANS, L.J., SCHOFIELD, J.T., MCCLEESE, D.J., MELBOURNE, W.G., THORNTON, C.L., YUNCK, T.P., EYRE, J.R., and NAGATANI, R.N., 1996, Initial results of radio occultation observations of Earth's atmosphere using the Global Positioning System, Science, **271**, 1107 – 1110.

KURSINSKI, E.R., HAJJ, G.A., SCHOFIELD, J.T., LINFIELD, R.P., and HARDY, K.R., 1997, Observing Earth's atmosphere with radio occultation measurements using the Global Positioning System, J. Geophys. Res., **102**, 23,429 – 23,465.

KURSINSKI, E.R., and HAJJ, G.A., 2001, A comparison of water vapor derived from GPS occultations and global weather analyses. J. Geophys. Res., **106**, 1113-1138.

KURSINSKI, E.R., HAJJ, G.A., LEROY, S.S., and HERMANN, B., 2000, The GPS Radio Occultation Technique. Terr. Atmos. and Ocean. Sci., **11**, pp. 53–114.

LEROY, S.S., 1997, Measurement of geopotential heights by GPS radio-occultation J. Geophys. Res., **102**, pp. 6971–6986.

ROCKEN, C., ANTHES, R., EXNER, M., HUNT, D., SOKOLOVSKIY, S., WARE, R., GORBUNOV, M., SCHREINER, W., FENG, D., HERMAN, B., KUO, Y.-H., and ZOU, X., 1997, Analysis and validation of GPS/MET data in the neutral atmosphere J. Geophys. Res., **102**, 29,849 – 29,866.

SYNDERGAARD, S., 2000, On the ionosphere calibration in GPS radio occultation measurements. Radio Science, **35**, pp. 865–883.

VOROB'EV, V.V., and KRASIL'NIKOVA, T.G., 1994, Estimation of the accuracy of the atmospheric refractive index recovery from Doppler shift measurements at frequencies used in the NAVSTAR system. Izvestiya Academy of Sciences, SSSR, Atmospheric and Oceanic Physics, English Translation, **29**, 5, 602–609.

WARE R., EXNER, M., FENG, D., GORBUNOV, M., HARDY, K., HERMAN, B., KUO, Y.-H., MEEHAN, T., MELBOURNE, W., ROCKEN, C., SCHREINER, W., SOKOLOVSKIY, S., SOLHEIM, F., ZOU, X., ANTHES, R., BUSINGER, S., and TRENBERTH, K., 1996, GPS sounding of the atmosphere from low Earth orbit - preliminary results. Bull. Amer. Meteor. Soc., **77**, pp. 19–40.

WU, S.C., YUNCK, T.P., and THORNTON, C.L., 1991. Reduced-dynamic technique for precise orbit determination of low earth satellites. J. Guid., Control and Dynamics, 14(1), 24-31.

YUNCK, T.P., LINDAL, G.F., LIU, C.H., 1988, The role of GPS in precise earth observation, paper presented at the IEEE Position, Location and Navigation symposium, Orlando, FL., Nov. 29-Dec. 2, 1988.

TABLES:

Vel Component	Mean	Std dev	Max dev
v_h (mm/s)	0.42	0.073	0.58
v_c (mm/s)	0.18	0.031	0.27
v_l (mm/s)	0.21	0.042	0.34

Table I: Mean, Standard deviation and Maximum deviation of the differences among velocity components of the orbit solutions over 31 days in 1995.

Year	Min(A_p)	Max(A_p)	$< A_p >$	$\sigma(A_p)$	Median(A_p)	Days with A_p = Median(A_p)
1995	1	100	12.65	11.32	8	22 (days)
1996	1	38	9.31	6.93	7	31 (days)
1997	0	59	8.41	7.89	6	37 (days)
1999	0	91	12.53	11.14	9	16 (days)
2000	1	164	15.08	17.16	10	19 (days)

Table II: Statistics of the global ionospheric variability in terms of the A_p index.

Polynom order	Mean	Std dev	Median	Max - Min
1	-0.513	42.16	-0.31	2053
2	8.131	397.91	0.076	44244
4	6.916	394.68	0.065	44197

Table III: Statistics of the differences in the phase rates (dual-single) for the calibrated signals using different polynomial expansions of the ionospheric correction. The statistics were accumulated for all the 1-sec points. The values are in mm/s.

FIGURE CAPTIONS:

Figures 1: (a) Mean values of the L2-SNR as a function of time over 1660 occultations for with the AS-off for GPS/MET in blue, and with the AS-on 273 for CHAMP in green, 1000 for GPS/MET in red, and 1000 for OERSTED in brown. (b) Ionospheric correction term for one occultation in 1995-06-22, during the AS-off period, of GPS/MET and 1996-05-06 during the AS-on period. Single (one per second) and dual (50 per second) values differ strongly during the AS-on period while they are close for the AS-off occultation. The phase bias B_k causes an indeterminate shift in the phase delay values. This shift was made zero by subtracting the first value on all curves.

Figures 2: Scatter plots of the differences between the time derivative of the phase delays. Dual minus single frequency phase rates of the calibrated signals are shown. (a) is for a linear model in the single frequency method and (b) is for a fourth degree polynomial expansion.

Figures 3: Refractivity N and Temperature T profiles for an occultation in 1995-05-03 using dual and single frequency methods.

Figures 4: Statistics of Fractional Refractivity N, and Temperature differences between the dual and single frequency retrievals as a function of height. Results for the 10 sec model windows are shown in open circles, while the results for 30 sec model windows are shown in close squares.

Figures 5: Statistics of Fractional Refractivity N, and Temperature differences between the single frequency and the ECMWF model. (occultation - model). (a) Mean and standard deviation of the refractivity differences. (b) Mean and standard deviation of the temperature differences.

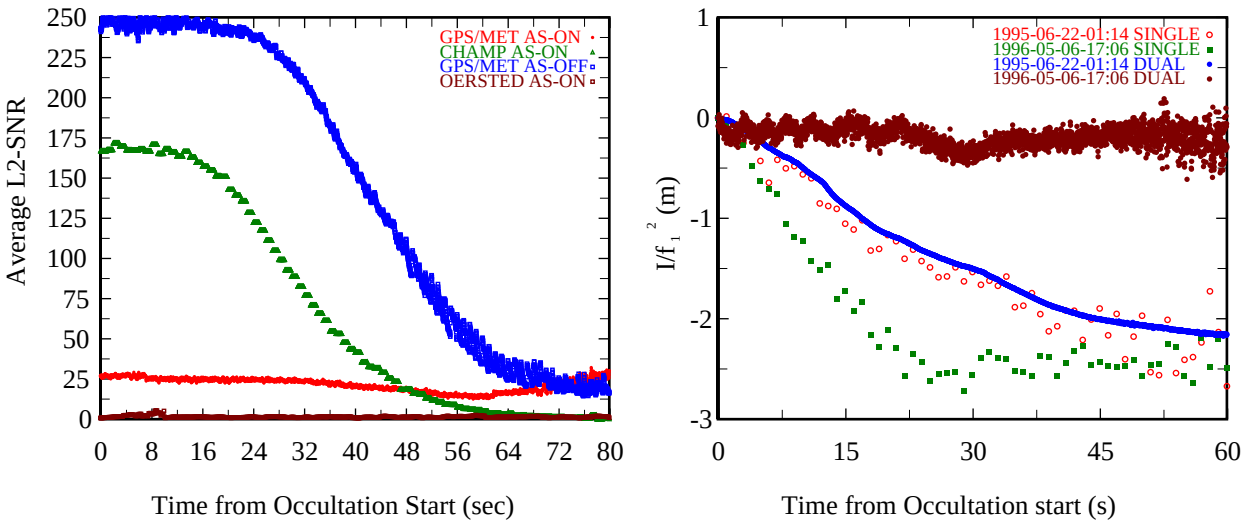

Figure 1: (a) Mean values of the L2-SNR as a function of time over 1660 occultations for with the AS-off for GPS/MET in blue, and with the AS-on 273 for CHAMP in green, 1000 for GPS/MET in red, and 1000 for OERSTED in brown. (b) Ionospheric correction term for one occultation in 1995-06-22, during the AS-off period, of GPS/MET and 1996-05-06 during the AS-on period. Single (one per second) and dual (50 per second) values differ strongly during the AS-on period while they are close for the AS-off occultation. The phase bias B_k causes an indeterminate shift in the phase delay values. This shift was made zero by subtracting the first value on all curves.

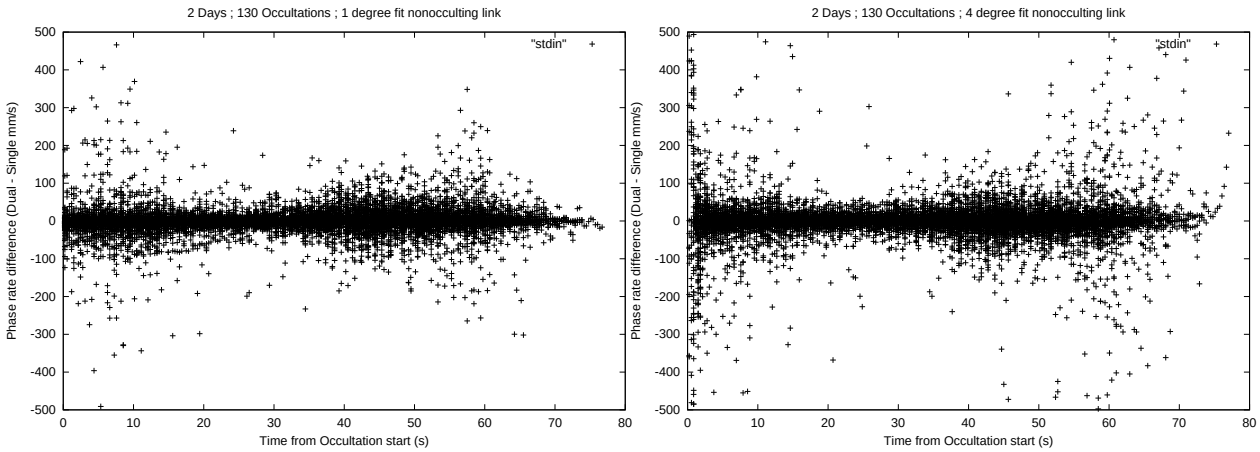

Figure 2: Scatter plots of the differences between the time derivative of the phase delays. Dual minus single frequency phase rates of the calibrated signals are shown. (a) is for a linear model in the single frequency method and (b) is for a fourth degree polynomial expansion.

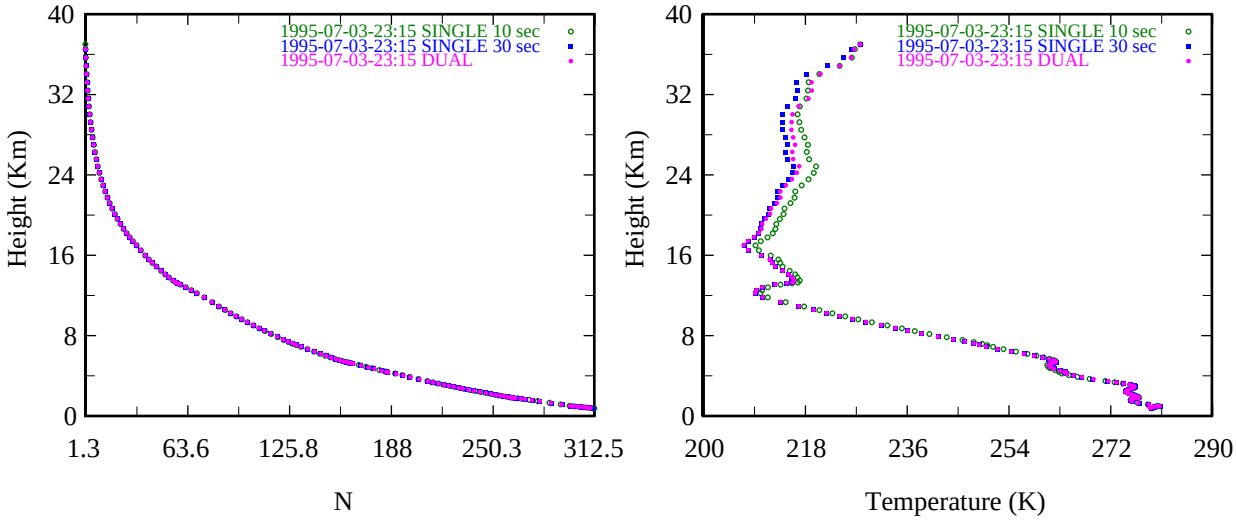

Figure 3: Refractivity N and Temperature T profiles for an occultation in 1995-05-03 using dual and single frequency methods.

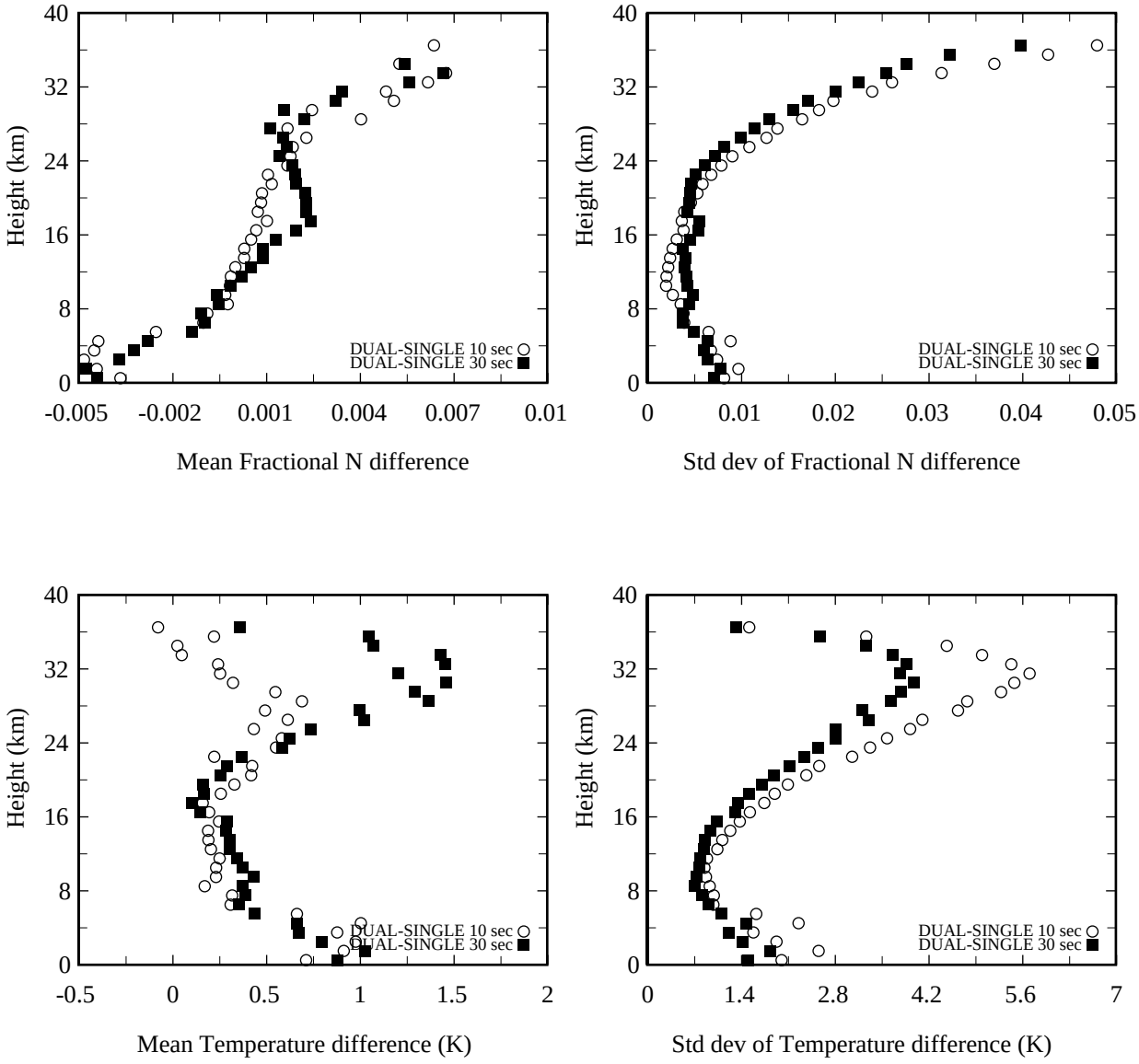

Figure 4: Statistics of Fractional Refractivity N, and Temperature differences between the dual and single frequency retrievals as a function of height. Results for the 10 sec model windows are shown in open circles, while the results for 30 sec model windows are shown in close squares.

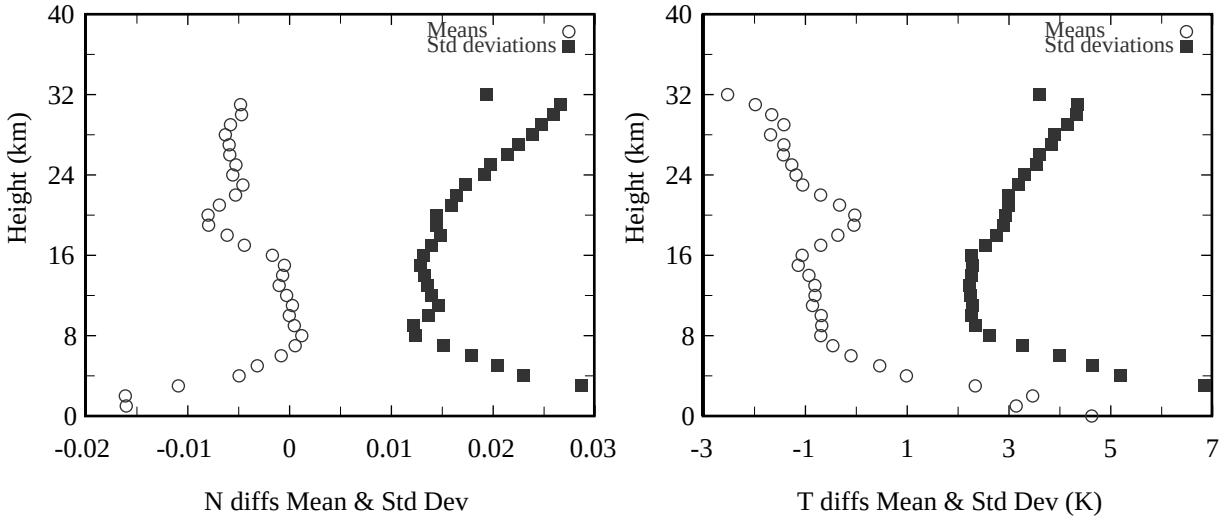

Figure 5: Statistics of Fractional Refractivity N, and Temperature differences between the single frequency and the ECMWF model (occultation - model). (a) Mean and standard deviation of the refractivity differences. (b) Mean and standard deviation of the temperature differences.